Forces Driving Chaperone Action

Graphical Abstract

Highlights

- Chaperone Spy is lured to client protein by electrostatic, not hydrophobic forces

- Client folding triggers its own release, making the chaperone self-regulating

- Client self-folding eliminates the need for client specific folding instructions

- This explains how chaperones can facilitate the folding of unrelated proteins
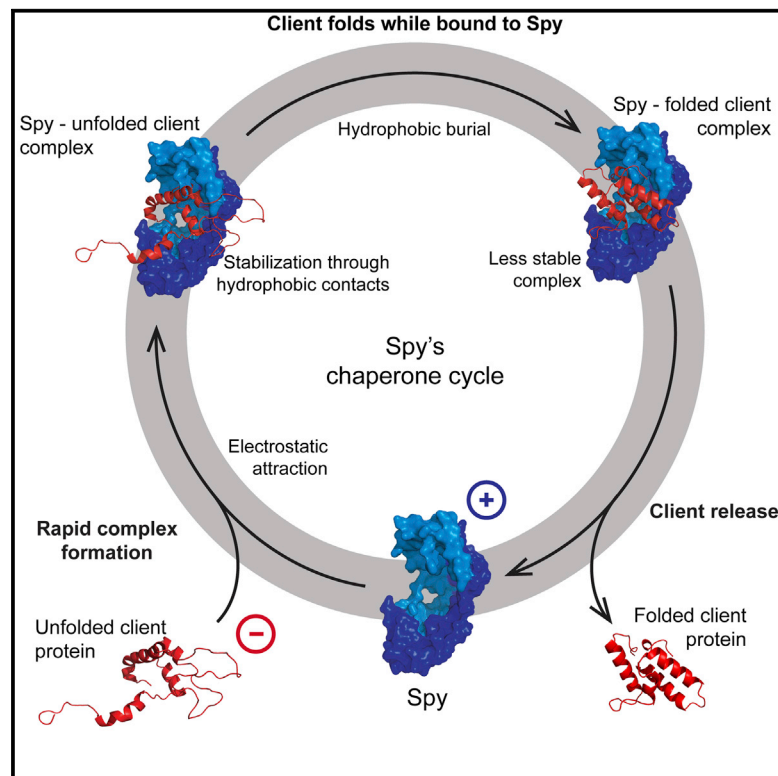
Authors

Philipp Koldewey, Frederick Stull, Scott Horowitz, Raoul Martin, James C.A. Bardwell

Correspondence

jbardwel@umich.edu

In Brief

A chaperone is lured to its unfolded client by electrostatic rather than hydrophobic interactions, and a sequential transition between these two forces promotes folding and release, all without ATP.

CellPress

Article

Forces Driving Chaperone Action

Philipp Koldewey,[1] Frederick Stull,[1] Scott Horowitz,[1] Raoul Martin,[1] and James C.A. Bardwell[1,*]
[1]Department of Molecular, Cellular and Developmental Biology, and the Howard Hughes Medical Institute, University of Michigan, Ann Arbor, MI 48109, USA
*Correspondence: jbardwel@umich.edu
http://dx.doi.org/10.1016/j.cell.2016.05.054

SUMMARY

It is still unclear what molecular forces drive chaperone-mediated protein folding. Here, we obtain a detailed mechanistic understanding of the forces that dictate the four key steps of chaperone-client interaction: initial binding, complex stabilization, folding, and release. Contrary to the common belief that chaperones recognize unfolding intermediates by their hydrophobic nature, we discover that the model chaperone Spy uses long-range electrostatic interactions to rapidly bind to its unfolded client protein Im7. Short-range hydrophobic interactions follow, which serve to stabilize the complex. Hydrophobic collapse of the client protein then drives its folding. By burying hydrophobic residues in its core, the client's affinity to Spy decreases, which causes client release. By allowing the client to fold itself, Spy circumvents the need for client-specific folding instructions. This mechanism might help explain how chaperones can facilitate the folding of various unrelated proteins.

INTRODUCTION

Molecular chaperones are fundamental to the cell, both in facilitating protein folding and in preventing cytotoxic protein aggregation, particularly during de novo protein synthesis and cellular stress. A relatively small set of chaperones is used to maintain the diverse array of proteins that are present in the cell. Chaperones have thus evolved to recognize and bind to a large variety of cellular proteins that differ not only in primary sequence, but also in their secondary and tertiary structure, and therefore in their folding state (Kim et al., 2013).

How chaperones recognize and select their client proteins has been an enigma since the beginning of research in this area. Based primarily on the most obvious structural characteristics of unfolded and unfolding client proteins, namely, the presence of exposed hydrophobic surfaces, it has become widely accepted that chaperones use hydrophobic interactions to recognize and bind to their clients (Clerico et al., 2015; Li et al., 2009; Saio et al., 2014). For some chaperones, such as GroEL, ATP binding and hydrolysis was found to trigger conformational changes in the client binding site that change the surface hydrophobicity and therefore allow the controlled binding and release of the client proteins

(Hayer-Hartl et al., 2016; Karagöz and Rüdiger, 2015; Li and Buchner, 2013; De Los Rios and Barducci, 2014; Saibil et al., 2013).

Aided by innovative genetic approaches, several new chaperones have recently been identified, some of which appear to promote the refolding of clients without any obvious means of regulating client binding and release (Huang et al., 2000; Jakob et al., 1993; Merz et al., 2006; Quan et al., 2011). These discoveries raise the obvious question as to how these chaperones recognize and bind client proteins in their unfolded conformation, maintain apparently stable complexes, and release client proteins once folded, all without the use of co-chaperones or other cofactors such as ATP.

Spy, a periplasmic protein of *Escherichia coli*, is a member of this new group of chaperones that promote client binding and folding without any obvious use of energy, cofactors, or post-translational modifications that might control the chaperone's conformation and client binding capacity. Spy's chaperone function was discovered by its ability to stabilize the protein Im7 in vivo (Quan et al., 2011). Spy is a highly effective molecular chaperone that allows Im7 to fold to completion while bound to it (Quan et al., 2011; Stull et al., 2016). The overall function of Spy thus appears to be to stabilize *Escherichia coli* periplasmic proteins from tannins and other agents that interfere with protein folding (Quan et al., 2011).

Im7 is a 10 kDa *E. coli* monomeric protein that has been used extensively to study protein folding. Moreover, conditions and mutants of Im7 have been developed that enable both partially and fully unfolded Im7 variants to remain soluble (Capaldi et al., 2001, 2002; Friel et al., 2009; Gsponer et al., 2006; Pashley et al., 2012; Whittaker et al., 2007). These Im7 variants therefore avoid aggregation, one of the major challenges in working with chaperone clients and a key reason that the number of kinetic and thermodynamic studies on chaperones is limited. Based on all these considerations and that both Spy and Im7 are very amenable to structural and biophysical approaches, we used this pair to address several fundamentally important questions concerning chaperone-client interactions. Here, we demonstrate that Spy initially uses long-range electrostatic interactions to rapidly bind to unfolded Im7. Following this initial encounter, hydrophobic contacts between Spy and unfolded Im7 form, which complement the electrostatics and stabilize the complex. The very amphiphilic nature of these interactions likely helps Im7 to explore its folding landscape while bound to Spy. Subsequent burial of Im7's hydrophobic residues during its folding process then reduces its binding affinity to Spy and self-regulates its release from the chaperone. These data describe how the interplay of molecular forces involved in chaperone action facilitate
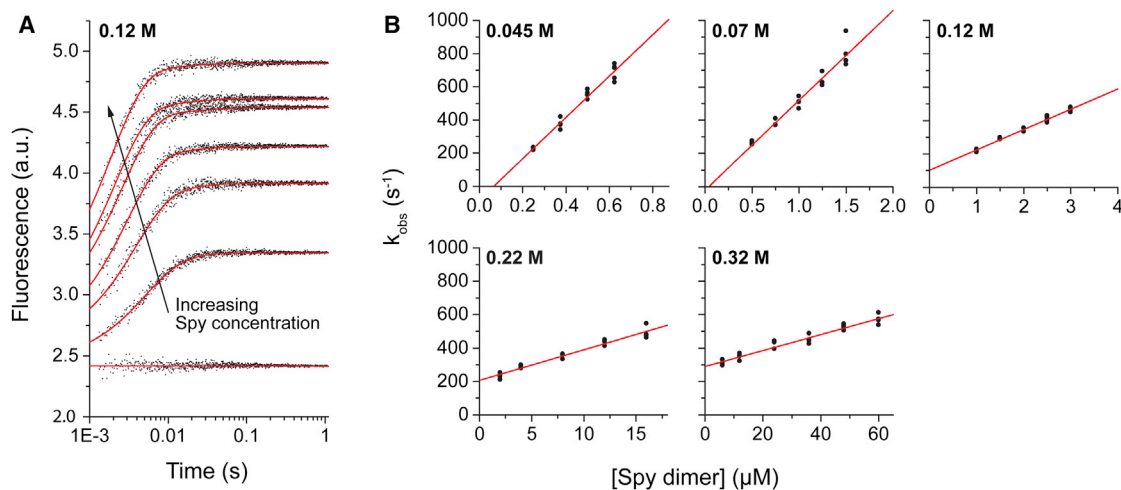
Figure 1. Complex Formation between Spy and Im7$_{A3W}$ Slows Down with Increasing Salt Concentrations as Determined by Stopped-Flow Fluorescence

(A) Representative raw transients for 250 nM Im7$_{A3W}$ mixed with increasing concentrations of Spy at an ionic strength of 0.12 M in the stopped-flow fluorimeter. Traces were fit with a double exponential function to obtain observed rate constants (k_{obs}). The kinetic traces are averages of four replicates.

(B) k_{obs} of the bimolecular step of Spy-Im7 interaction were plotted as a function of Spy dimer concentration to determine the binding (k_{on}) and release (k_{off}) rate constant at increasing ionic strengths and 22°C: 0.0625 μM Im7$_{A3W}$ (0.045 M), 0.125 μM Im7$_{A3W}$ (0.07 M), 0.250 μM Im7$_{A3W}$ (0.12 M), 0.5 μM Im7$_{A3W}$ (0.22 M), and 1.5 μM Im7$_{A3W}$ (0.32 M) were mixed with increasing concentrations of Spy$_{WT}$. k_{obs} at low ionic strength (< 0.12 M) were derived from single exponential fits of the raw fluorescence transients, whereas at ionic strength $\geq$ 0.12 M, double exponential fits were used (see Figure S3). A linear fit of k_{obs} as a function of Spy concentration yielded k_{on} from the slope and k_{off} from the intercept (Table S1). At an ionic strength of 0.12 M, Spy binds to Im7$_{A3W}$ with a k_{on} of 1.2 ± 0.4 × 10^8 M^{-1}s^{-1}, which is consistent with what was shown for the interaction of Spy with Im7$_{A3}$ (Stull et al., 2016), demonstrating that the tryptophan substitution does not affect the kinetics of Spy-Im7 interaction. The ionic strength was adjusted with sodium chloride in 40 mM HEPES (pH 7.5). The k$_{obs}$ of four experiment per Spy concentration were plotted to show the experimental error.

client binding, folding, and release, without the need for allosteric regulation of the chaperone.

RESULTS

Electrostatic Interactions Enhance Spy-Client Binding

The biophysically amenable nature of the recently discovered chaperone Spy and one of its in vivo clients, Im7, together with the previously established mechanism of Im7 folding (Capaldi et al., 2001, 2002; Friel et al., 2009; Gsponer et al., 2006; Pashley et al., 2012; Whittaker et al., 2007), afforded us the opportunity to analyze the forces governing how an unfolded protein binds, folds, and is subsequently released by a chaperone.

We previously showed that Spy binds its unfolded client protein Im7 very rapidly, with a rate constant of 1.3 ± 0.2 × 10^7 M^{-1}s^{-1} (Stull et al., 2016). This fast binding rate constant is consistent with previous studies on the interaction kinetics of chaperones such as GroEL, SecB, and trigger factor with their clients, which have also been shown to be rapid diffusion-controlled processes (Fekkes et al., 1995; Maier et al., 2001; Perrett et al., 1997). The rate constant for Spy-client interaction is about two to three orders of magnitude faster than the average basal association rate constants for bio-macromolecules, which are ~10^5–10^6 M^{-1}s^{-1} (Berg and von Hippel, 1985; Schreiber et al., 2009). While extremely rapid association rates help to explain how chaperones effectively compete with protein aggregation, the chemical forces that drive these processes are unclear. We considered two primary mechanisms

that would enhance protein-protein interactions above the basal association rate: long-range electrostatic interactions and an induced fit mechanism that invokes a generation of a higher affinity binding site upon initial encounter (Pontius, 1993; Schreiber et al., 2009; Shoemaker et al., 2000; Wright and Dyson, 2009).

We analyzed the kinetics of Spy-client complex formation by stopped-flow fluorescence measurements in buffers containing various concentrations of sodium chloride (25 to 300 mM) to alter the ionic strength. We reasoned that if electrostatic forces were indeed involved in complex formation, the bimolecular rate constant should decline exponentially with increasing ionic strength due to screening of the charges on the two interacting proteins (Schreiber et al., 2009; Selzer and Schreiber, 1999; Vijayakumar et al., 1998).

Since Spy does not contain any tryptophan residues, we used the tryptophan fluorescence of Im7 to monitor chaperone-client complex formation via stopped-flow. To mimic the unfolded state of Im7, we used the Im7 variant Im7 L18AL19AL37AH40W (hereafter termed Im7$_{A3W}$), which is fully unfolded, soluble, and binds Spy tightly in a 1:1 ratio under native conditions (see Figures S1 and S2) (Pashley et al., 2012; Stull et al., 2016). As shown previously, Spy binding to Im7$_{A3W}$ causes an increase in tryptophan fluorescence (Stull et al., 2016), which we fitted to exponential functions to obtain an observed rate constant (k_{obs}) (Figures 1A and S3). Analysis of the k_{obs} in buffers of increasing ionic strengths revealed a linear dependence on Spy concentration under all salt conditions, indicating that the observed increase in fluorescence in these experiments corresponds to
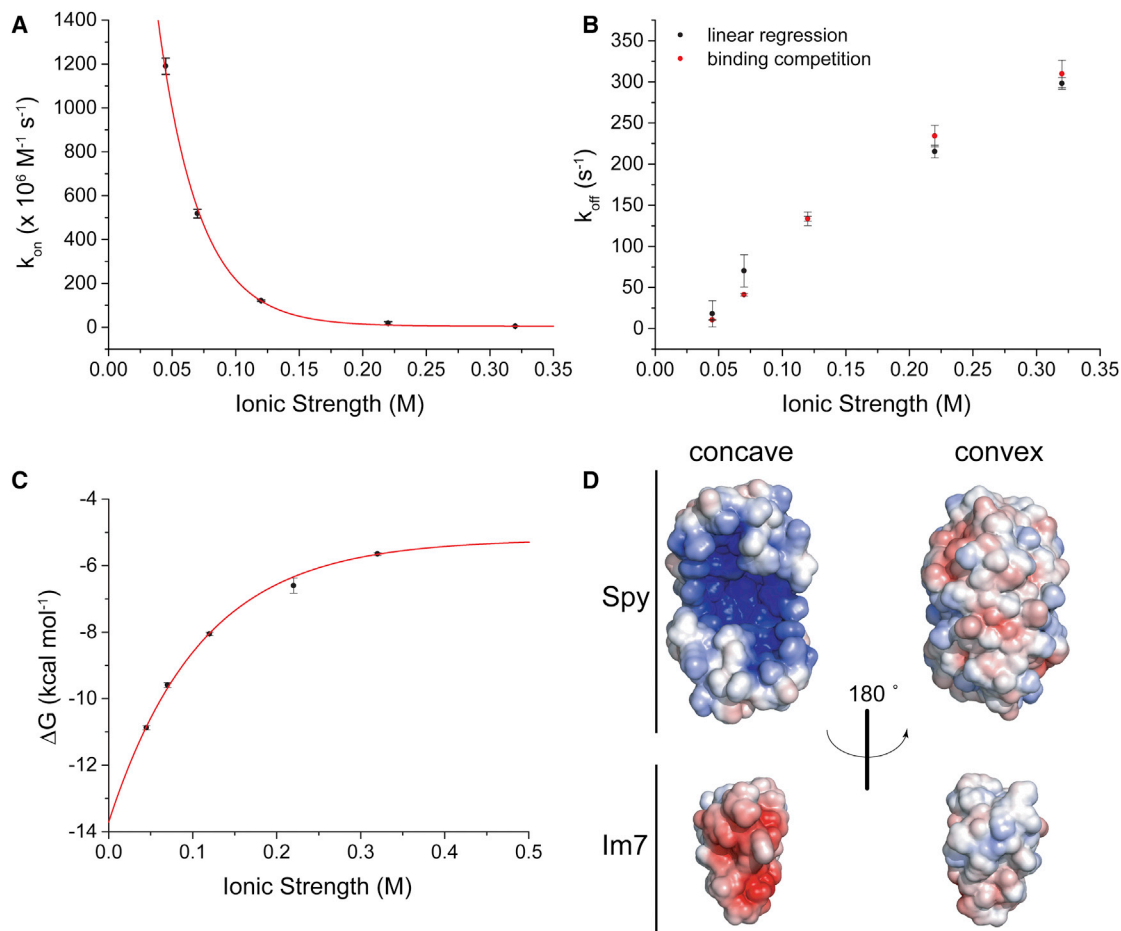
Figure 2. Spy-Im7$_{A3W}$ Binding Is Salt-Dependent

(A and B) Stopped-flow binding experiments were conducted in 40 mM HEPES, pH 7.5 of different ionic strengths, adjusted with 0.025 to 0.30 M sodium chloride (see Figure 1).

(A) The binding rate constant k_{on} of Spy-Im7$_{A3W}$ interaction as a function of ionic strength was derived from the slope of the linear fits of the observed rate constants (see Figure 1B). Errors are propagated fitting standard errors of four independent data points.

(B) The release rate constant k_{off} was derived either from the corrected y-intercepts of linear fits (black, see Figure 1B) or competition experiments (red) (see Figure S3). The binding and release rate constants are affected differently by the ionic strength. Whereas k_{on} decreases exponentially with increasing ionic strength (A), k_{off} increases exponentially (B). Note that at all ionic strengths tested, the release rate constant obtained by binding competition is, within error, identical to the k_{off} determined from the corrected y-intercept. Errors are propagated fitting standard errors of four independent data points.

(C) The binding free energy (ΔG) of Spy-Im7$_{A3W}$ interaction increases exponentially with ionic strength. The ΔG was derived from the kinetic dissociation constant (K_d) (see Table S1). At infinite ionic strength, when all electrostatic interactions are screened, $\Delta G = -5.2$ kcal mol^{-1}, suggesting that hydrophobic interactions contribute to complex stability. Errors are propagated fitting standard errors of three independent data points.

(D) Distribution of positive and negative surface charge on Spy (PDB: 3O39) and folded Im7 (PDB: 1CEI). Whereas positive charges (blue) outweigh negative charges (red) on the concave side of Spy, the convex side reveals a more even charge distribution. In contrast, Im7 contains a hot-spot of condensed negative charge at the site where it binds to its in vivo binding partner E7 (Ko et al., 1999). The electrostatic surface potential was calculated via PyMol using the APBS tools2.1 plugin (a color scale for the charge distribution from −5 to 5 was chosen). The respective .pqr file was generated on the PDB2PQR website for a pH of 7.5 (http://www.poissonboltzmann.org) (Unni et al., 2011).

the bimolecular step of Spy binding to Im7$_{A3W}$ (Figures 1B and S3). Importantly, we found that k_{obs} is highly dependent on the ionic strength of the buffer and decreased at each Spy concentration as the ionic strength increased. Next, we fitted k_{obs} as a function of Spy concentration to a line and determined the binding rate constant (k_{on}) from the slope for each ionic strength (Figure 1B). We found that k_{on} decreased exponentially with increasing salt concentration, indicating that electrostatic forces

are an important component of client binding to Spy (Figure 2A and Table S1).

Fitting a plot of k_{on} against the ionic strength with an exponential function allowed us to determine the boundaries of the binding rate constant at high and low ionic strength, respectively (Figure 2A). At very low ionic strength (i.e., equivalent to 1 mM), the maximum binding rate constant was determined to be 4.5×10^9 M^{-1}s^{-1}. This rate constant is very close to the

theoretical maximal diffusion-limited association rate constant between Spy and $Im7_{A3W}$, which was calculated to be $5 \times 10^9 \ M^{-1}s^{-1}$ at this temperature (see Experimental Procedures), implying that this is a diffusion-limited, orientation independent binding process. At the limit of high salt concentration (> 0.5 M), the association rate constant was found to be three orders of magnitude lower ($4.5 \times 10^6 \ M^{-1}s^{-1}$). This latter rate constant is in line with those commonly observed for protein-protein interactions that are not electrostatically enhanced (Schreiber et al., 2009). Thus, at physiological salt concentrations (e.g., in the human large intestine, where the ionic strength is between 0.1 and 0.165 M; Kararli, 1995), electrostatic attractions between Im7 and Spy enhance the binding rate constant by at least two orders of magnitude. Spy is expressed at extremely high levels following stress, reaching concentrations as high as 2.7 mM (Quan et al., 2011). Given that the binding rate constant with Im7 ranges from 3×10^7 to $2 \times 10^8 \ M^{-1}s^{-1}$ at physiological salt, the binding half time with Im7 would be 1.2 to 7.7 μsec, very likely fast enough to efficiently compete with aggregation. We also tested the salt dependence of the binding kinetics with two previously characterized in vitro Spy clients, casein and reduced carboxymethylated α-lactalbumin (Quan et al., 2011, 2014). As observed for Im7, k_{on} decreased exponentially with increasing ionic strength, indicating that binding enhancement through electrostatic attraction is a common feature of Spy-client complexes (Figure S4).

Spy possesses an overall positive charge (isoelectric point of 9.47), whereas Im7 exhibits an overall negative charge (isoelectric point of 4.37) (Pashley et al., 2012) (Figure 2D). To rule out the possibility that the observed interaction between Spy and its clients is simply due to non-specific electrostatic interactions, we conducted isothermal titration calorimetry (ITC) binding experiments between $Im7_{A3W}$ and RNase A, a 13.7 kDa protein whose size and isoelectric point are similar to those of Spy (isoelectric point of 8.64). As shown in Figure S5A, we did not observe any measurable interaction between these two proteins, indicating that the binding of Spy to $Im7_{A3W}$ is not just due to non-specific electrostatic interactions between two oppositely charged proteins.

Client Release from Spy Is Less Sensitive to Ionic Strength than Is Binding

To investigate how client release is affected by the ionic strength, we determined the release rate constant (k_{off}) from both the y-intercept of the binding plots and by performing binding competition experiments (see Figures 1B and S3). In contrast to k_{on}, which decreases ~250-fold over the range of ionic strengths tested, k_{off} only increased by ~30-fold (Figures 2A and 2B and Table S1). While this result demonstrates that electrostatic interactions are also important for maintaining the Spy-$Im7_{A3W}$ complex, they appear to play a more critical role in complex formation. Such differences in the ionic strength dependence of binding and release rate constants have been reported for a number of other protein-protein interactions (Darling et al., 2002; Hemsath et al., 2005; Joachimiak et al., 2014; Radić et al., 1997; Schreiber and Fersht, 1993; Wallis et al., 1995; Zhou, 2001, 2003). Our results suggest that the forces governing unfolded Im7 binding and release are at least partially different.

Whereas the formation of the complex is strongly affected by long-range electrostatic forces, other intermolecular forces are involved in stabilizing the complex.

While we have evidence that electrostatic interactions are an important component in chaperone-client recognition and binding, we cannot entirely exclude that an induced fit mechanism may also contribute to the rapid binding reaction. Folding of Im7, which can occur while bound to Spy (Stull et al., 2016), can easily be imagined to accelerate complex formation. In the case of an intrinsically disordered protein client, the folding that occurs upon complex formation generally acts to stabilize the complex (Bardwell and Jakob, 2012; Wright and Dyson, 2009). In the case of Spy, however, stabilization seems rather counterproductive, as this would result in the folded state of the client binding with higher affinity than the unfolded state. Thus, the folded client protein would tend to be trapped on the surface of the chaperone. Indeed, we observed that the folded state of Im7 binds with the lower affinity than unfolded Im7 (Stull et al., 2016). These observations argue against the induced fit model.

Spy-Client Release Is Controlled by Hydrophobic Interactions

How can binding of the client be more affected by ionic strength than its release? One possible explanation is that binding may involve interactions that are not present in the final complex; i.e., the initial, electrostatically mediated encounter complex may relax into an ensemble that involves fewer charged residues. This ensemble could then be stabilized through other forces, such as hydrophobic interactions. To investigate which forces play a role in complex stability and how they contribute to chaperone function, we next investigated the role that hydrophobic interactions play in the Spy-Im7 complex.

Previous studies revealed that some gain of function mutations (termed Super Spy variants) in Spy that improved chaperone activity in the *E. coli* periplasm increased the hydrophobic surface on Spy's concave side and increased its affinity for Im7 by up to six-fold (Quan et al., 2014). These results suggested that hydrophobic residues are involved in Spy-client interactions. To test whether the increased Im7 affinity for Super Spy variants was due to changes in client binding or release, we investigated the interaction of $Im7_{A3W}$ with the two most active Super Spy variants, Q100L (Spy_{Q100L}) and H96L (Spy_{H96L}), via stopped-flow fluorescence. Both of the mutated residues in these variants are located on the interior of the concave side of Spy and therefore increase its hydrophobicity (Quan et al., 2014). Since wild-type Spy (Spy_{WT}) binds Im7 with a rate already near the theoretical limit and hydrophobic interactions are short-ranged, we hypothesized that increased client-chaperone binding rate constants could not explain the superior chaperone activity of these Super Spy variants. Indeed, the association rate constants of Spy_{Q100L} and Spy_{H96L} did not differ dramatically from that of Spy_{WT} (Figure 3 and Table S1), suggesting that the interaction of these Spy variants with $Im7_{A3W}$ is primarily guided by electrostatically-driven client recognition. While Spy_{H96L}-$Im7_{A3W}$ association could be fit by a single exponential function, Spy_{Q100L} displayed two additional phases (Figures S3F and S3G). Both additional phases were found to be independent of the Spy_{Q100L}
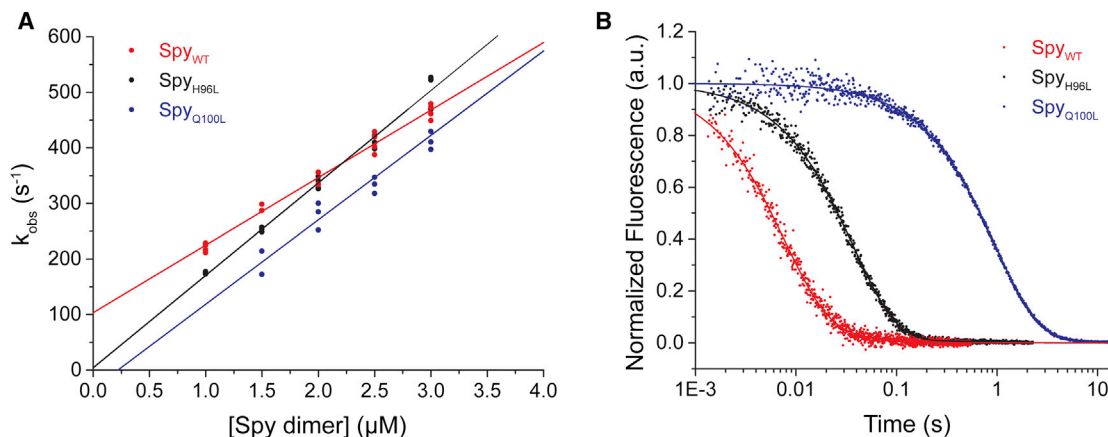
Figure 3. Super Spy Variants Q100L and H96L Bind Im7$_{A3W}$ Tighter than Spy$_{WT}$ Due to a Slower Release Rate Constant

(A) Observed rate constants (k_{obs}) of the binding step were derived from single (Spy$_{H96L}$) double (Spy$_{WT}$) or triple (Spy$_{Q100L}$) exponential fits of the raw transients (Figure S3) and are plotted as a function of Spy concentration: 0.25 μM Im7$_{A3W}$ mixed with Spy$_{WT}$, 1st phase (red), Spy$_{H96L}$ (black), or Spy$_{Q100L}$, 1st phase (blue). Data were fit to a line to yield the binding rate constant of Spy to Im7 (see Table S1). Three independent data points per Spy concentration were collected to show the experimental error. Note that the k_{obs} of the additional phases can be found in Figure S3.

(B) Binding competition experiments in which 0.25 μM Im7$_{A3W}$ in complex with the respective Spy variant (2 μM Spy$_{WT}$ (red), 2 μM Spy$_{H96L}$ (black), 0.5 μM Spy$_{Q100L}$ (blue)) was mixed with the tryptophan-free, unfolded Im7 variant, Im7$_{A3W75F}$ (see also Figure S3). All traces show a small second phase and had to be fit to a double exponential function. The kinetic traces are averages of four replicates.

All experiments were performed in 40 mM HEPES, pH 7.5, 100 mM sodium chloride. See also Table S1.

concentration (Figures S3L and S3M), implying that these two phases correspond to unimolecular steps. Since Spy$_{Q100L}$ is a better chaperone than Spy$_{WT}$ (Quan et al., 2014), these unimolecular steps could involve Spy-induced Im7$_{A3W}$ folding. In either case, we concluded that increased association rates do not explain the enhanced chaperone activity of these Super Spy variants and that hydrophobic interactions are not a major driving force for the initial complex formation.

To determine the rates at which the two Super Spy variants release their clients, we performed the same binding competition experiments that we employed for Spy$_{WT}$. In these experiments, we first formed complexes between Spy and Im7$_{A3W}$ and then mixed these complexes with the tryptophan-free variant Im7$_{A3W75F}$ to compete for Spy's client binding site. We found the Im7$_{A3W}$ release rate constants of Spy$_{H96L}$ and Spy$_{Q100L}$ to be, respectively, 5- and 130-fold lower than that of Spy$_{WT}$ (Figures 3B and S3 and Table S1), explaining the ~7- and 150-fold increase in client affinity of the Super Spy variants. Our finding that Spy variants with increased surface hydrophobicity show decreased client release rates strongly suggests that surface hydrophobicity is an important component of complex stability and primarily controls the client release rate.

Hydrophobic Desolvation Manifests in Entropic Complex Stabilization

To understand, from a thermodynamic point of view, how the interplay of hydrophobic and electrostatic forces drives complex formation and stability, we conducted ITC experiments and directly determined binding enthalpy (ΔH), binding entropy (ΔS), and the K_d. The ITC experiments clearly showed that complex formation between all tested Spy variants and the unfolded client Im7$_{A3W}$ is an endothermic process and therefore must be entirely entropically driven (Figures 4A and S5B–S5D and Table

S1). Performing ITC binding titrations at various salt concentrations revealed the expected increase in the K_d as the ionic strength of the buffer increased, consistent with our kinetic data (Figure 2C and Table S1). Intriguingly, however, we found that whereas the entropy of the reaction remained unchanged throughout the salt concentration range tested, the enthalpy exponentially increased with ionic strength, leveling off only at high salt concentrations (Figure 5). Since salt ions screen electrostatic interactions but do not substantially weaken hydrophobic interactions, this finding suggests that the observed entropy gain upon binding is a result of desolvation of hydrophobic surface residues. The increase in enthalpy with ionic strength reflects the contribution of intermolecular salt bridges in the binding reaction, as the formation of salt bridges is an exothermic process (Matulis and Lovrien, 1998). These results are consistent with our conclusion that hydrophobic interactions play a minor role for the initial Spy-Im7$_{A3W}$ complex formation, but constitute the major force in complex stabilization. Thus, chaperone-client complex stability likely comes from hydrophobic shielding, reconciling some apparently contradictory models as to how chaperones function (Katsumata et al., 1996; Kim et al., 2013).

To directly determine whether hydrophobic shielding dominates the entropic stabilization of the Spy-Im7$_{A3W}$ complex, we measured the heat capacity change (ΔC_p) upon complex formation by analyzing the temperature dependence of ΔH_b (Figures 4B and S6). The magnitude and the sign of ΔC_p are directly correlated with the surface area that is being solvated or desolvated upon complex formation (Prabhu and Sharp, 2005). Desolvation of hydrophobic surface area results in a negative ΔC_p, whereas desolvation of hydrophilic residues produces a positive ΔC_p. The net change is proportional to the summed contributions to ΔC_p by hydrophilic and hydrophobic surface areas involved in the binding interface. The interaction of Spy$_{WT}$
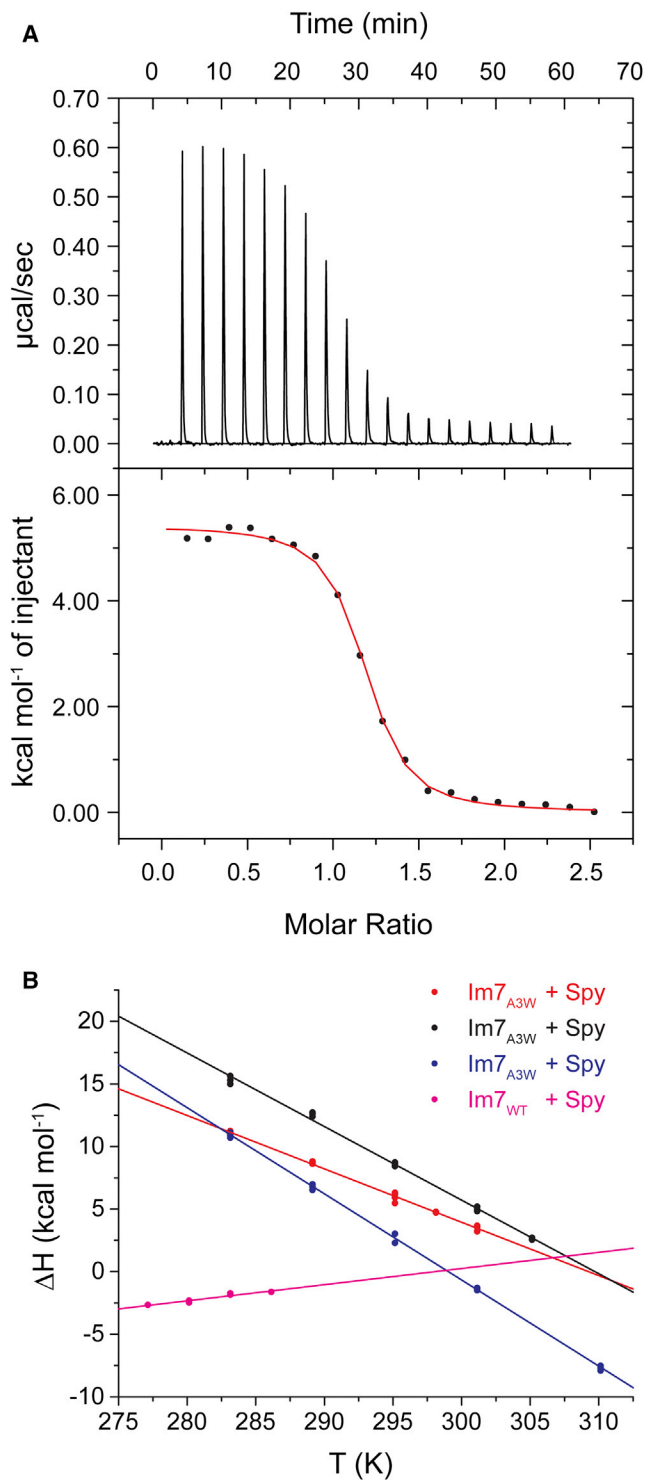
A

B

Figure 4. Spy-Im7 Interaction Is an Entropy-Driven Process Due to Hydrophobic Interactions in the Complex

(A) Representative ITC binding isotherm of Spy_{WT} + $Im7_{A3W}$ at 22°C. Integrated thermograms (bottom graph) are fit to a single site-binding model.

(B) Binding enthalpy (ΔH) of Spy-Im7 complex formation as a function of temperature measured via ITC. The heat capacity changes (ΔC_p) were derived from the slope of a linear fit. $Im7_{A3W}$ binding to Spy_{WT} (red), Spy H96L (black),
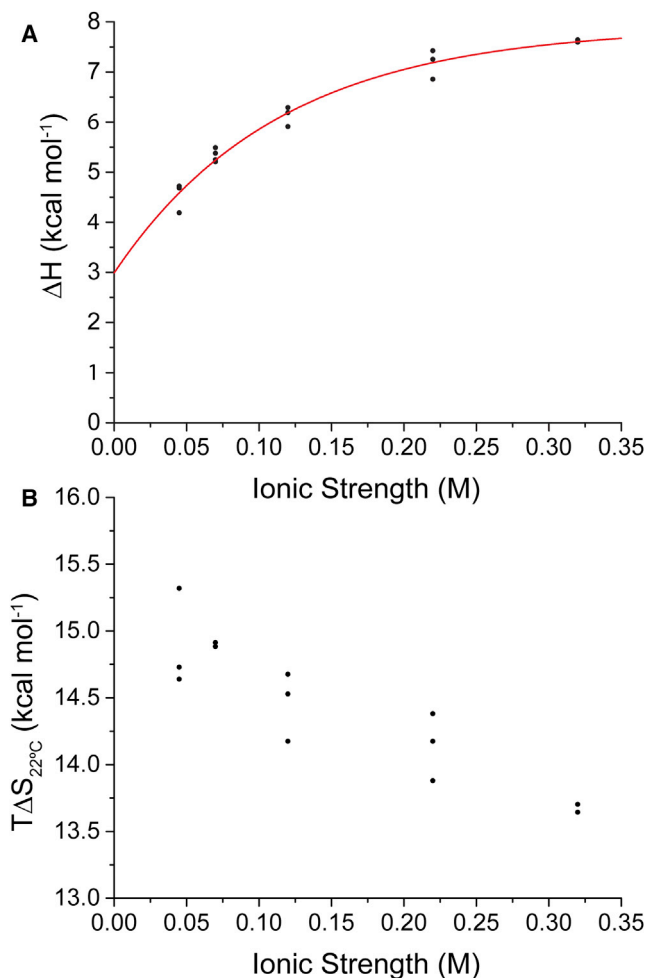
A

B

Figure 5. Screening of Ionic Interactions Enthalpically Disfavors Complex Formation

(A and B) ITC binding titrations of Spy-$Im7_{A3W}$ with Spy_{WT} at 22°C were performed in 40 mM HEPES (pH 7.5) containing 25 to 300 mM sodium chloride to obtain thermodynamic parameters: enthalpy (ΔH) (A) and entropy (ΔS) (B). Three independent data points per sodium chloride concentration were collected to show the experimental error.

with $Im7_{A3W}$ resulted in a strongly negative ΔC_p of -426 ± 8 cal mol^{-1}K^{-1} (Figure 4B). Even more negative ΔC_p values of -588 ± 11 and -688 ± 6 cal mol^{-1}K^{-1} were observed for the Super variants Spy_{H96L} and Spy_{Q100L}, respectively (Figure 4B). These results strongly support the conclusion that the entropic stabilization of the Spy-$Im7_{A3W}$ complex is a result of desolvation of hydrophobic surface area upon binding.

Although the Spy-Im7 complex is primarily entropically stabilized, the K_d does not significantly change throughout the temperature range tested (Figure S6C). This invariance is due to the change in entropy being compensated by an enthalpy

or Spy Q100L (blue) resulted in a negative ΔC_p, whereas $Im7_{WT}$ titrated with Spy_{WT} (magenta) resulted in a positive ΔC_p. All experiments were performed in 40 mM HEPES (pH 7.5), 100 mM sodium chloride. Three independent data points per Spy concentration were collected to show the experimental error.
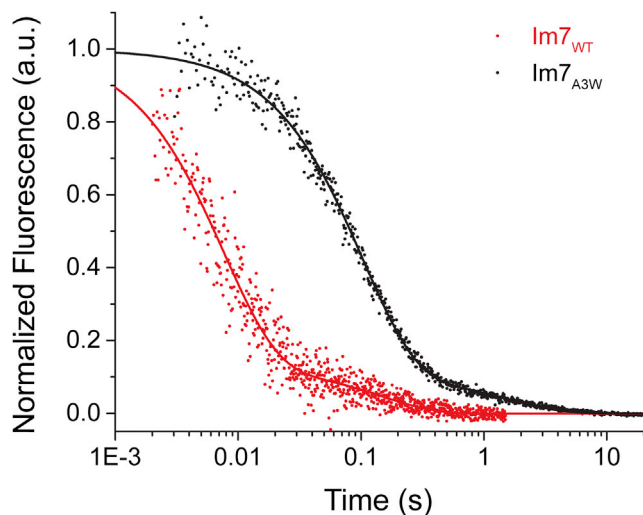
Figure 6. Native State of Im7 Is Released from Spy 13-Fold Faster than the Unfolded State

Binding competition experiments were performed: 2.5 μM Im7$_{WT}$ in complex with 4 μM Spy$_{WT}$ dimer was mixed with 50 μM of Im7$_{A3W75F}$ to determine the release rate constant of natively folded Im7 (red); 0.25 μM Im7$_{A3W}$ in complex with 0.5 μM Spy$_{WT}$ dimer was mixed with 25 μM of Im7$_{A3W75F}$ to determine the release rate constant of the unfolded state of Im7 (black). In both cases, a double exponential fit was used (see also Figure S7). The second, slow phase observed for Im7$_{WT}$ is caused by either refolding or release of a subpopulation of partially unfolded Im7$_{WT}$, whereas the fast phase is due to the release of the bound native state of Im7, as revealed by double mixing experiments (see Figure S7). This experiment was performed at 4°C in 40 mM HEPES (pH 7.5) and 25 mM sodium chloride to slow down the release of Im7$_{WT}$. The kinetic traces are averages of four replicates.

change in the opposite direction (Figure S6D). Enthalpy-entropy compensation has been reported for numerous protein complexes as a way for biological systems to tolerate a broader range of environmental temperatures (Cooper et al., 2001; Kabiri and Unsworth, 2014; Liu et al., 2000). *E. coli*, and many other prokaryotic organisms containing Spy, are able to grow over a wide range of temperatures (for *E. coli* this range is 14°C–48°C) (Herendeen et al., 1979) and can be subject to unfolding stresses (e.g., tannin exposure) at all of these temperatures. As a result, Spy is likely needed over the entire temperature growth range of *E. coli*. The enthalpy-entropy compensation for Spy-client binding could be a way for Spy to remain functional over the range of temperatures encountered by *E. coli*.

Im7 Folding Breaks Hydrophobic Contacts with Spy

The experiments with the constitutively unfolded Im7$_{A3W}$ revealed that client release of unfolded Im7 is primarily controlled by hydrophobic contacts. In addition, we know that folding of Im7 occurs while bound to Spy (Stull et al., 2016). Since Im7 folding buries hydrophobic residues within its own core, these two observations taken together raised the intriguing possibility that Im7 folding itself could trigger its release from Spy. To determine if folding of Im7 indeed disrupts the hydrophobic interactions between Spy and Im7, we analyzed the interaction of Spy with folded Im7$_{WT}$ using ITC. Measuring the temperature dependence of ΔH_b for natively folded Im7$_{WT}$ binding to Spy revealed a

clearly positive ΔC_p of 129 ± 2 cal mol^{-1}K^{-1}, in stark contrast to the very negative ΔC_p observed for the unfolded variants of Im7 (Figure 4B). This result suggests that once the client was folded, the complex was no longer stabilized by hydrophobic interactions. Thus, Im7 folding appears to change the underlying properties of the complex by breaking intermolecular hydrophobic contacts with Spy and weakening binding (Table S1).

Natively Folded Im7 Is Released from Spy Faster than Unfolded Im7

To test whether the loss of intermolecular hydrophobic contacts triggers Im7 release upon folding, we determined the release rate constant of Im7$_{WT}$ from Spy. We recently showed that Spy binds the native state of Im7, although with a lower affinity than the unfolded state (Stull et al., 2016). Since the release of Im7$_{WT}$ from Spy is too fast to be observed by stopped-flow even at 10°C, we were unable to directly determine the k_{off} for the Im7$_{WT}$-Spy complex (Stull et al., 2016). We thus performed competition experiments with the Im7$_{WT}$-Spy complex using our tryptophan-free competitor Im7$_{A3W75F}$ at 4°C and low ionic strength (to slow down the dissociation of native Im7 from Spy) (Figures 6 and S7D). This competition experiment revealed two phases, with observed rate constants of 131 ± 7 s^{-1} and 6.4 ± 1.5 s^{-1}, with the faster phase contributing ~90% of the total signal change. Recent work showed that Spy's high affinity to unfolded Im7 causes fully folded Im7$_{WT}$ to partially unfold upon binding to Spy at 10°C (Stull et al., 2016). At 4°C, we also observed some minor Spy-induced unfolding which is likely responsible for the biphasic character of the release rate (Figure S7B and Table S1). Hence, one of the two phases observed in the competition experiment may actually be reporting on the release and/or refolding of the small amount of unfolded Im7 bound to Spy. To determine which of the two phases is due to the release of the native state of Im7 and which is due to the partial unfolding, we performed double-mixing experiments. We first mixed Im7$_{WT}$ with Spy to allow for complex formation. After 6 ms, we chased the reaction with our competitor Im7$_{A3W75F}$ (Figure S7E). We picked 6 ms because at this point of the reaction, Im7$_{WT}$ is fully bound to Spy but no partial unfolding of Im7 has occurred (Figure S7B); thus, only the dissociation of native Im7 from Spy should be observed. Indeed, when we chased our complexes with the competitor after 6 ms, the slow phase disappeared, whereas the fast phase remained (k_{obs} 141 ± 4 s^{-1}). These experiments demonstrate that the major fast phase is due to the release of natively folded Im7 from Spy (Figures 6, S7D, and S7E and Table S1). We also performed competition experiments with the Im7$_{A3W}$-Spy complex at 4°C so we could directly compare the release rate constants of unfolded and native Im7 from Spy under the same conditions (Figures 6, S7F, and S7G). Whereas Im7$_{A3W}$ dissociates from Spy with a rate constant of 10 ± 1 s^{-1}, Im7$_{WT}$ is released with a rate constant of 131 ± 7 s^{-1}. The faster release of native Im7 is consistent with its weaker binding affinity to Spy compared to the other Im7 folding states (Stull et al., 2016). The ~13-fold increased k_{off} for the folded state over the unfolded state demonstrates that folding of Im7 and subsequent hydrophobic burial drives Im7's release from Spy due to the lack of intermolecular hydrophobic interactions.
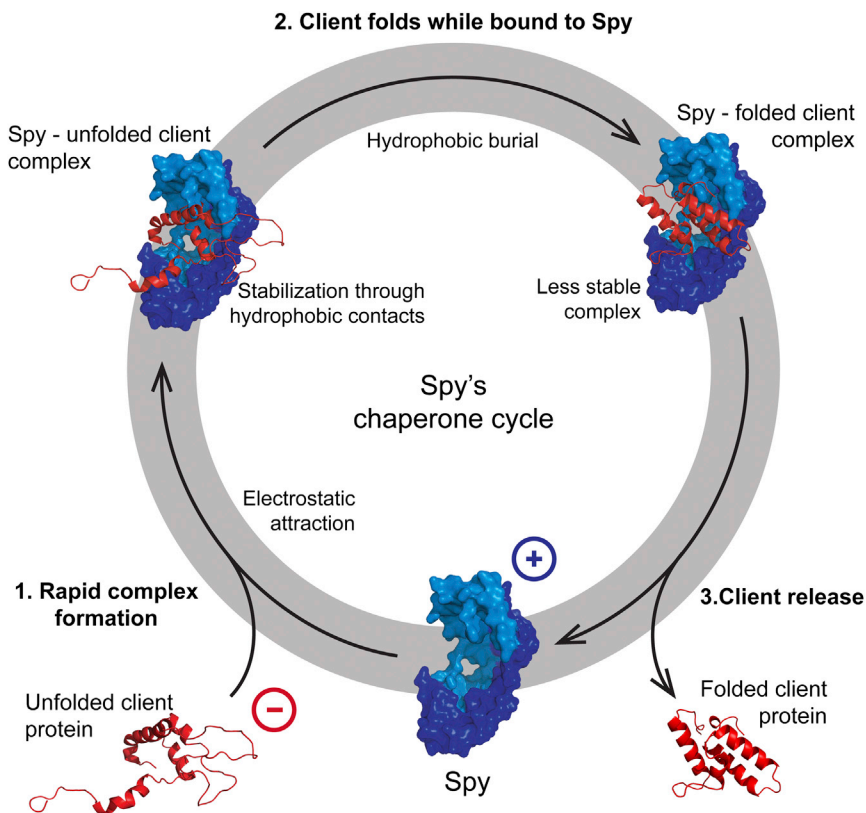
2. Client folds while bound to Spy

Figure 7. Mechanistic Scheme of Spy-Client Interaction
(1) Client binding rates are maximized through long-range electrostatic attraction, which allows Spy (blue) to effectively compete with aggregation of the unfolded client protein (red). Client release, on the other hand, is energetically disfavored mainly by the solvation of hydrophobic surface area on the client and Spy, which are buried in the complex. (2) Folding of the client results in the burial of hydrophobic residues in the client's core, which decreases its affinity to Spy, and therefore (3) favors release of the client protein. The electrostatic interactions, however, allow the client to stay bound to Spy while it folds.

reducing the hydrophobic component of complex stability. The complex therefore becomes less stable, resulting in an increased release rate of the now folded client from Spy. Thus, folding of the client protein drives its release from the chaperone. Our data provide a nuanced understanding of how molecular interactions and protein folding can direct the binding, folding, and release of client proteins from a self-regulated ATP- and co-chaperone independent molecular chaperone (Figure 7). The mechanism of protein folding while associated with a chaperone proposed here relies upon a change in surface properties of the protein as it folds. Interestingly, mass spectroscopy studies have suggested that the net charge on the protein surface may decrease for some proteins upon folding. The controversy over this topic was recently reviewed (Hall and Robinson, 2012). Future studies on if and how the surface charge of proteins changes upon folding in the presence and absence of chaperones could provide useful insight into the interactions between chaperones and clients.

That electrostatic interactions play such an important role in chaperone-client binding might seem counterintuitive, since chaperones are known to bind to exposed hydrophobic surface areas of un- or misfolded client proteins. This gives rise to the common conception that chaperone binding is driven by hydrophobic interactions (Hartl et al., 2011). However, electrostatic interactions are better poised to rapidly reduce the concentration of aggregation-sensitive folding intermediates because they are longer in range, and therefore can increase binding rates to a greater extent than shorter-range hydrophobic interactions can (Schreiber et al., 2009; Selzer and Schreiber, 1999; Vijayakumar et al., 1998). Moreover, electrostatics have also been postulated to be important for client-recognition by other chaperones such as GroEL, Hsp90, Hsp70, CCT, and Hsp33 (Hagn et al., 2011; Joachimiak et al., 2014; Kasper et al., 2000; Liu et al., 2003; Perrett et al., 1997; Reichmann et al., 2012). Similarly, we have recently shown that polyanions such as RNA, DNA and polyphosphate are very effective ATP-independent chaperones (Docter et al., 2016; Gray et al., 2014). While the molecular

DISCUSSION

From our experimental results on Spy-Im7 interactions, we can construct a model for how this chaperone interacts with its clients. It appears that Spy binds to and releases client proteins in a regulated fashion that uses client protein folding as its own cue for release. The high density of positive charges on Spy's client-binding site allows for a directed and very rapid binding of unfolded negatively charged proteins in the periplasm, *and* most periplasmic proteins are negatively charged (Heidary et al., 2014). After the initial encounter complex, hydrophobic interactions form between Spy and the unfolded client protein, which entropically stabilize the complex and result in a shielding of exposed hydrophobic surface on the client. The mixture of electrostatic and hydrophobic residues on Spy's surface may provide what we call a "folding friendly" surface that allows the client to explore its folding landscape (Stull et al., 2016). Very recently, we developed a crystallographic approach to visualize dynamic and heterogeneous proteins that enabled us to determine an ensemble depicting Im7 folding while bound to Spy (Horowitz et al., 2016). The ensemble suggests that specific electrostatic interactions between Spy and Im7 could help tether Im7 to the surface of Spy during the folding process. The chaperone Spy thus allows the client protein to fold itself, circumventing the need for client-specific folding instructions. This mechanism may help explain how chaperones can facilitate the folding of various unrelated proteins.

The folding of the client protein while bound to Spy results in burial of hydrophobic residues within the interior of the client,

forces driving the chaperone function of these polyanions have not yet been characterized, it is plausible that electrostatic forces are vital to these highly charged molecules' chaperone activity.

We speculate that providing a folding friendly surface that allows client proteins to fold themselves may be a general property of foldase chaperones. Most notably, the heterogeneous interior surface of the eukaryotic GroEL homolog CCT/TRiC was previously postulated to be important in its protein-folding capability (Joachimiak et al., 2014). Similarly, a recent structural analysis of Hsp90-Tau binding found that the Hsp90 client interaction site contained a mixture of hydrophobic and charged residues (Karagöz et al., 2014), with superficially similar properties to the mixed hydrophobic and charged folding surface of Spy. It is possible that the interactions between folding proteins and these ATP-dependent chaperones change from hydrophobic to hydrophilic during the folding process, as observed here for Spy. It has long been known, for instance, that GroEL initially binds client in a hydrophobic manner, but following GroES association, large rigid body movements change the interior of the GroEL cavity to a hydrophilic surface (Hayer-Hartl et al., 2016; Saibil et al., 2013). Similar as for Spy, folding-friendly surfaces may allow other chaperones to escape the need to provide client specific folding instructions by allowing the client to direct their own folding. The simple folding surface strategy employed by Spy presumably evolutionarily preceded more elaborate ATP driven chaperones. It is possible that the addition of ATP dependence through evolution does not fundamentally alter this underlying self-folding mechanism, but instead provides a layer of regulation that allows ATP-dependent chaperones to better control client binding and release to facilitate folding. Spy's heterogeneous folding surface perhaps lies evolutionarily part-way between primordial chaperones like nucleic acids and well studied but complex and energy dependent chaperone machines such as Hsp90 and GroEL/S.

EXPERIMENTAL PROCEDURES

Stopped-Flow Fluorescence and Data Fitting

Previously, we used a tryptophan fluorescence-based stopped-flow approach to determine the binding rate constant (k_{on}) and the release rate constant (k_{off}) of Im7$_{A3}$ binding to Spy (Stull et al., 2016). To analyze the effects of ionic strength on the two microscopic rate constants, we chose the same approach; however, in this case, we used the unfolded variant Im7$_{A3W}$, taking advantage of the environmental sensitivity of the additional tryptophan residue (see also Supplemental Experimental Procedures). The transient kinetics of Spy-client complex formation were recorded using a SF-2004 stopped-flow spectrofluorimeter (KinTek) by monitoring the change in tryptophan fluorescence of the Im7$_{A3W}$ or Im7$_{WT}$ upon addition of Spy$_{WT}$ or the Spy variants H96L and Q100L. As before (Stull et al., 2016), we detected an increase in tryptophan fluorescence upon addition of Spy to Im7$_{A3W}$ (Figures 1A and S3) and fitted the transients to exponential functions to derive observed rate constants (k_{obs}). To determine the binding rate constant (k_{on}), Im7$_{A3W}$ or Im7$_{WT}$ was mixed with increasing concentrations of the respective Spy variant at a flow rate of 8 ml s^{-1}. The tryptophan was excited at 296 nm and fluorescence emission was recorded using a 340 ± 10 nm bandpass filter. Monochromator slits were set to 4 nm each. All experiments were carried out at 4°C or 22°C in 40 mM HEPES (pH 7.5) and different amounts of sodium chloride to investigate the salt dependence of the binding reaction. The final concentration after mixing of Im7$_{A3W}$ and Spy was chosen such that a pseudo-first-order approximation could be used for the data analysis and the observed rate constants did not exceed the limits of the instrument (the dead time was determined to be 1.3 ms): 62.5 nM Im7$_{A3W}$ at 25 mM sodium chloride, 125 nM Im7$_{A3W}$ at 50 mM sodium chloride,

250 nM Im7$_{A3W}$ at 100 mM sodium chloride, 500 nM Im7$_{A3W}$ at 200 mM sodium chloride, and 1.5 μM Im7$_{A3W}$ at 300 mM sodium chloride. At 4°C in 40 mM HEPES, 100 mM sodium chloride, 2.5 μM Im7$_{WT}$ was titrated with sub-stoichiometric quantities of Spy to obtain a binding isotherm for the native state of Im7 since binding was too fast to be observed by stopped-flow.

Binding competition experiments using stopped-flow fluorescence were conducted to determine the release rate constant (k_{off}) from different Spy variants as well as under different salt concentrations. The same amount of Im7$_{A3W}$ at the salt concentration indicated above was premixed with 250 nM Spy$_{WT}$ dimer (25 mM sodium chloride), 500 nM Spy$_{WT}$ dimer (50 mM sodium chloride), 2 μM Spy$_{WT}$ dimer, Spy$_{H96L}$, or 500 nM Spy$_{Q100L}$ (100 mM sodium chloride), 8 μM Spy$_{WT}$ dimer (200 mM sodium chloride), or 24 μM Spy$_{WT}$ dimer (300 mM sodium chloride). The formed complex was then loaded into the stopped-flow instrument and mixed with tryptophan-free Im7$_{A3W75F}$ (tryptophan 75 in Im7$_{A3}$ was replaced by a phenylalanine; see also Supplemental Experimental Procedures) as a competitor for Spy's client binding site, up to a concentration after which no more change in the observed rate constant could be detected: 6.25 μM Im7$_{A3W75F}$ (25 mM sodium chloride), 25 μM Im7$_{A3W75F}$ (50 mM sodium chloride), 50 μM Im7$_{A3W75F}$ (100 mM sodium chloride, Spy$_{WT}$), 75 μM Im7$_{A3W75F}$ (100 mM sodium chloride, Spy$_{H96L}$), 100 μM Im7$_{A3W75F}$ (100 mM sodium chloride, Spy$_{Q100L}$), 300 μM Im7$_{A3W75F}$ (200 mM sodium chloride), and 900 μM Im7$_{A3W75F}$ (300 mM sodium chloride).

To determine the binding rate constant (k_{on}), all transients of the Spy-client interaction collected by stopped-flow were fitted with a single, double, or triple exponential function (for Spy$_{Q100L}$). The observed rate constants (k_{obs}) derived from the exponential fit were then plotted as a function of Spy concentration. Phases that showed an increasing linear dependence of k_{obs} on Spy concentration were fitted with a linear function to obtain k_{on} using the equation below (Kozlov and Lohman, 2002):

$$k_{obs} = k_{on} * [\text{Spy}] + k_{off} - k_{on} * [\text{Im7}_{A3W}]$$

For Im7$_{A3W}$ binding to Spy$_{WT}$ as well as Spy$_{Q100L}$ at an ionic strength $\geq$ 0.12 M we observed one to two minor, slow phases in addition to the fast major phase which corresponded to the binding step. These slower phases appeared to be invariant to the Spy concentration (Figures S3H–S3J), indicating that this phase corresponds to a unimolecular step that either precedes or follows Spy binding to Im7$_{A3W}$. Thus, this slow phase observed at high ionic strengths could represent the partial folding of Im7$_{A3W}$ upon binding to Spy. However, since it contributed less than 10% of the total signal change, causing a wide range of variability in k_{obs} of these slow phases, we only analyzed k_{obs} of the first, major phase.

The dissociation constant (k_{off}) was calculated either from the y-intercept of linearly fitted observed rate constants of the major phase or determined via binding competition with Im7$_{A3W75F}$ (see above). In the latter case, the raw data were fitted with a double exponential function. All errors are illustrated by either plotting the individual data points of at least three independent experiments or are averages of propagated standard errors of the data fits.

Double-mixing binding competition experiments with Im7$_{WT}$ or Im7$_{A3W}$ and Spy$_{WT}$ were performed in 40 mM HEPES (pH 7.5), 25 mM sodium chloride at 4°C by first mixing a final concentration of 2.5 μM Im7$_{WT}$ with 4 μM Spy$_{WT}$ or 0.25 μM Im7$_{A3W}$ with 0.75 μM Spy$_{WT}$ to allow for complex formation. After 6 ms (Im7$_{WT}$) or 10 ms (Im7$_{A3W}$), the reaction was chased with 50 μM (Im7$_{WT}$) or 25 μM (Im7$_{A3W}$) tryptophan free Im7$_{A3W75F}$. The recorded transients were fit with a single exponential function.

Theoretical Diffusion-Limited Association Rate Constant

The theoretical, diffusion-limited binding rate constant ($k_{encounter}$) of Spy and Im7$_{A3W}$ was calculated using the Smoluchowski equation below (von Hippel and Berg, 1989):

$$k_{encounter} = 4 * \pi (D_S + D_I) * (r_S + r_I) * \frac{N_0}{1000}$$

where D_S and D_I are the diffusion coefficients of Spy and Im7$_{A3W}$, r_S and r_I are the hydrodynamic radii of the Spy dimer and Im7, and N_0 is Avogadro's

number. Diffusion coefficients were obtained by analytical ultracentrifugation (Figure S2A and Supplemental Experimental Procedures), and the hydrodynamic radius for both proteins was calculated from the crystal structure of Im7 (PDB: 1CEI) and Spy (PDB: 3O39) using the program HYDROPRO (Ortega et al., 2011).

ITC

ITC was performed using a MicroCal iTC200 (Malvern Instruments) with Im7 in the cell and Spy in the titration syringe. All samples were dialyzed against the respective buffer overnight prior to running the experiment. Concentrations of Spy dimer or RNaseA (110–3600 μM in the syringe) and Im7 (10–300 μM in the cell) were varied depending on the K_d of the binding reaction at the respective condition. Injection volumes of 1–2 μl and injection intervals of 120 to 600 s were used. The solution was stirred at 1,000 rpm and the reference power was set to 6 μcal s^{-1} in high feedback mode. ITC thermograms were fit to a one-site model using the Origin software (OriginLab) provided with the instrument.

Salt dependence was determined by dialyzing samples against 40 mM HEPES (pH 7.5) containing 25 mM, 50 mM, 100 mM, 200 mM, or 300 mM sodium chloride, and performing experiments at 4°C or 22°C. Temperature dependence was determined by dialyzing samples against 40 mM HEPES (pH 7.5) containing 100 mM sodium chloride and performing experiments at temperatures ranging from 4°C to 37°C.

The change in heat capacity (ΔC_p) upon Spy-client complex formation was derived from the slope of a linear fit of the enthalpy change (ΔH) as a function of temperature [5] (Baldwin, 1986):

$$\Delta H°(T_2) = \Delta H°(T_1) + \Delta C_p * (T_2 - T_1)$$

where T is the absolute temperature. ΔC_p was assumed to be temperature independent. ΔH values of Im7$_{WT}$ titrated with Spy could only be collected at low temperatures (4°C–13°C), as previously shown, Im7$_{WT}$ partially unfolds when mixed with Spy (Stull et al., 2016). At temperatures from 4°C to 13°C, little to no unfolding was observed, and the percentage of partial unfolding increased with temperature exponentially (data not shown).

SUPPLEMENTAL INFORMATION

Supplemental Information includes Supplemental Experimental Procedures, seven figures, and one table and can be found with this article online at http://dx.doi.org/10.1016/j.cell.2016.05.054.

REFERENCES

Baldwin, R.L. (1986). Temperature dependence of the hydrophobic interaction in protein folding. Proc. Natl. Acad. Sci. USA 83, 8069–8072.

Bardwell, J.C., and Jakob, U. (2012). Conditional disorder in chaperone action. Trends Biochem. Sci. 37, 517–525.

Berg, O.G., and von Hippel, P.H. (1985). Diffusion-controlled macromolecular interactions. Annu. Rev. Biophys. Biophys. Chem. 14, 131–160.

Capaldi, A.P., Shastry, M.C.R., Kleanthous, C., Roder, H., and Radford, S.E. (2001). Ultrarapid mixing experiments reveal that Im7 folds via an on-pathway intermediate. Nat. Struct. Biol. 8, 68–72.

Capaldi, A.P., Kleanthous, C., and Radford, S.E. (2002). Im7 folding mechanism: misfolding on a path to the native state. Nat. Struct. Biol. 9, 209–216.

Clerico, E.M., Tilitsky, J.M., Meng, W., and Gierasch, L.M. (2015). How hsp70 molecular machines interact with their substrates to mediate diverse physiological functions. J. Mol. Biol. 427, 1575–1588.

Cooper, A., Johnson, C.M., Lakey, J.H., and Nöllmann, M. (2001). Heat does not come in different colours: entropy-enthalpy compensation, free energy windows, quantum confinement, pressure perturbation calorimetry, solvation and the multiple causes of heat capacity effects in biomolecular interactions. Biophys. Chem. 93, 215–230.

Darling, R.J., Kuchibhotla, U., Glaesner, W., Micanovic, R., Witcher, D.R., and Beals, J.M. (2002). Glycosylation of erythropoietin affects receptor binding kinetics: role of electrostatic interactions. Biochemistry 41, 14524–14531.

De Los Rios, P., and Barducci, A. (2014). Hsp70 chaperones are non-equilibrium machines that achieve ultra-affinity by energy consumption. eLife 3, e02218.

Docter, B.E., Horowitz, S., Gray, M.J., Jakob, U., and Bardwell, J.C.A. (2016). Do nucleic acids moonlight as molecular chaperones? Nucleic Acids Res. Apr. 21, gkw291.

Fekkes, P., den Blaauwen, T., and Driessen, A.J.M. (1995). Diffusion-limited interaction between unfolded polypeptides and the Escherichia coli chaperone SecB. Biochemistry 34, 10078–10085.

Friel, C.T., Smith, D.A., Vendruscolo, M., Gsponer, J., and Radford, S.E. (2009). The mechanism of folding of Im7 reveals competition between functional and kinetic evolutionary constraints. Nat. Struct. Mol. Biol. 16, 318–324.

Gray, M.J., Wholey, W.Y., Wagner, N.O., Cremers, C.M., Mueller-Schickert, A., Hock, N.T., Krieger, A.G., Smith, E.M., Bender, R.A., Bardwell, J.C., and Jakob, U. (2014). Polyphosphate is a primordial chaperone. Mol. Cell 53, 689–699.

Gsponer, J., Hopearuoho, H., Whittaker, S.B.-M., Spence, G.R., Moore, G.R., Paci, E., Radford, S.E., and Vendruscolo, M. (2006). Determination of an ensemble of structures representing the intermediate state of the bacterial immunity protein Im7. Proc. Natl. Acad. Sci. USA 103, 99–104.

Hagn, F., Lagleder, S., Retzlaff, M., Rohrberg, J., Demmer, O., Richter, K., Buchner, J., and Kessler, H. (2011). Structural analysis of the interaction between Hsp90 and the tumor suppressor protein p53. Nat. Struct. Mol. Biol. 18, 1086–1093.

Hall, Z., and Robinson, C.V. (2012). Do charge state signatures guarantee protein conformations? J. Am. Soc. Mass Spectrom. 23, 1161–1168.

Hartl, F.U., Bracher, A., and Hayer-Hartl, M. (2011). Molecular chaperones in protein folding and proteostasis. Nature 475, 324–332.

Hayer-Hartl, M., Bracher, A., and Hartl, F.U. (2016). The GroEL-GroES Chaperonin Machine: A Nano-Cage for Protein Folding. Trends Biochem. Sci. 41, 62–76.

Heidary, S., Rahim, R.A., Eissazadeh, S., Moeini, H., Chor, A.L.T., and Abdullah, M.P. (2014). Proteome analysis of Escherichia coli periplasmic proteins in response to over-expression of recombinant human interferon α2b. Biotechnol. Lett. 36, 1479–1484.

Hemsath, L., Dvorsky, R., Fiegen, D., Carlier, M.-F., and Ahmadian, M.R. (2005). An electrostatic steering mechanism of Cdc42 recognition by Wiskott-Aldrich syndrome proteins. Mol. Cell 20, 313–324.

Herendeen, S.L., VanBogelen, R.A., and Neidhardt, F.C. (1979). Levels of major proteins of Escherichia coli during growth at different temperatures. J. Bacteriol. 139, 185–194.

Horowitz, S., Salmon, L., Koldewey, P., Ahlstrom, L.S., Martin, R., Quan, S., Afonine, P.V., van den Bedem, H., Wang, L., Xu, Q., et al. (2016). Visualizing chaperone-assisted protein folding. NSMB. published online on May 30, 2016. http://dx.doi.org/10.1038/nsmb.3237.

Huang, G.C., Li, Z.Y., Zhou, J.M., and Fischer, G. (2000). Assisted folding of D-glyceraldehyde-3-phosphate dehydrogenase by trigger factor. Protein Sci. 9, 1254–1261.

Jakob, U., Gaestel, M., Engel, K., and Buchner, J. (1993). Small heat shock proteins are molecular chaperones. J. Biol. Chem. 268, 1517–1520.

Joachimiak, L.A., Walzthoeni, T., Liu, C.W., Aebersold, R., and Frydman, J. (2014). The structural basis of substrate recognition by the eukaryotic chaperonin TRiC/CCT. Cell 159, 1042–1055.

Kabiri, M., and Unsworth, L.D. (2014). Application of isothermal titration calorimetry for characterizing thermodynamic parameters of biomolecular interactions: peptide self-assembly and protein adsorption case studies. Biomacromolecules 15, 3463–3473.

Karagöz, G.E., and Rüdiger, S.G.D. (2015). Hsp90 interaction with clients. Trends Biochem. Sci. 40, 117–125.

Karagöz, G.E., Duarte, A.M.S., Akoury, E., Ippel, H., Biernat, J., Morán Luengo, T., Radli, M., Didenko, T., Nordhues, B.A., Veprintsev, D.B., et al. (2014). Hsp90-Tau complex reveals molecular basis for specificity in chaperone action. Cell 156, 963–974.

Kararli, T.T. (1995). Comparison of the gastrointestinal anatomy, physiology, and biochemistry of humans and commonly used laboratory animals. Biopharm. Drug Dispos. 16, 351–380.

Kasper, P., Christen, P., and Gehring, H. (2000). Empirical calculation of the relative free energies of peptide binding to the molecular chaperone DnaK. Proteins 40, 185–192.

Katsumata, K., Okazaki, A., Tsurupa, G.P., and Kuwajima, K. (1996). Dominant forces in the recognition of a transient folding intermediate of alpha-lactalbumin by GroEL. J. Mol. Biol. 264, 643–649.

Kim, Y.E., Hipp, M.S., Bracher, A., Hayer-Hartl, M., and Hartl, F.U. (2013). Molecular chaperone functions in protein folding and proteostasis. Annu. Rev. Biochem. 82, 323–355.

Radić, Z., Kirchhoff, P.D., Quinn, D.M., Mccammon, J.A., and Taylor, P. (1997). Electrostatic influence on the kinetics of ligand binding to acetylcholinesterase. Distinctions between active center ligands and fasciculin. J. Biol. Chem. 272, 23265–23277.

Ko, T.P., Liao, C.C., Ku, W.Y., Chak, K.F., and Yuan, H.S. (1999). The crystal structure of the DNase domain of colicin E7 in complex with its inhibitor Im7 protein. Structure 7, 91–102.

Kozlov, A.G., and Lohman, T.M. (2002). Stopped-flow studies of the kinetics of single-stranded DNA binding and wrapping around the Escherichia coli SSB tetramer. Biochemistry 41, 6032–6044.

Li, J., and Buchner, J. (2013). Structure, function and regulation of the hsp90 machinery. Biomed. J. 36, 106–117.

Li, Y., Gao, X., and Chen, L. (2009). GroEL recognizes an amphipathic helix and binds to the hydrophobic side. J. Biol. Chem. 284, 4324–4331.

Liu, L., Yang, C., and Guo, Q.X. (2000). A study on the enthalpy-entropy compensation in protein unfolding. Biophys. Chem. 84, 239–251.

Liu, W., Bratko, D., Prausnitz, J.M., and Blanch, H.W. (2003). Electrostatic interactions between peptides and the molecular chaperone DnaK. J. Phys. Chem. B 107, 11563–11569.

Maier, R., Scholz, C., and Schmid, F.X. (2001). Dynamic association of trigger factor with protein substrates. J. Mol. Biol. 314, 1181–1190.

Matulis, D., and Lovrien, R. (1998). 1-Anilino-8-naphthalene sulfonate anion-protein binding depends primarily on ion pair formation. Biophys. J. 74, 422–429.

Merz, F., Hoffmann, A., Rutkowska, A., Zachmann-Brand, B., Bukau, B., and Deuerling, E. (2006). The C-terminal domain of Escherichia coli trigger factor represents the central module of its chaperone activity. J. Biol. Chem. 281, 31963–31971.

Ortega, A., Amorós, D., and García de la Torre, J. (2011). Prediction of hydrodynamic and other solution properties of rigid proteins from atomic- and residue-level models. Biophys. J. 101, 892–898.

Pashley, C.L., Morgan, G.J., Kalverda, A.P., Thompson, G.S., Kleanthous, C., and Radford, S.E. (2012). Conformational properties of the unfolded state of Im7 in nondenaturing conditions. J. Mol. Biol. 416, 300–318.

Perrett, S., Zahn, R., Stenberg, G., and Fersht, A.R. (1997). Importance of electrostatic interactions in the rapid binding of polypeptides to GroEL. J. Mol. Biol. 269, 892–901.

Pontius, B.W. (1993). Close encounters: why unstructured, polymeric domains can increase rates of specific macromolecular association. Trends Biochem. Sci. 18, 181–186.

Prabhu, N.V., and Sharp, K.A. (2005). Heat capacity in proteins. Annu. Rev. Phys. Chem. 56, 521–548.

Quan, S., Koldewey, P., Tapley, T., Kirsch, N., Ruane, K.M., Pfizenmaier, J., Shi, R., Hofmann, S., Foit, L., Ren, G., et al. (2011). Genetic selection designed to stabilize proteins uncovers a chaperone called Spy. Nat. Struct. Mol. Biol. 18, 262–269.

Quan, S., Wang, L., Petrotchenko, E.V., Makepeace, K.A., Horowitz, S., Yang, J., Zhang, Y., Borchers, C.H., and Bardwell, J.C. (2014). Super Spy variants implicate flexibility in chaperone action. eLife 3, e01584.

Reichmann, D., Xu, Y., Cremers, C.M., Ilbert, M., Mittelman, R., Fitzgerald, M.C., and Jakob, U. (2012). Order out of disorder: working cycle of an intrinsically unfolded chaperone. Cell 148, 947–957.

Saibil, H.R., Fenton, W.A., Clare, D.K., and Horwich, A.L. (2013). Structure and allostery of the chaperonin GroEL. J. Mol. Biol. 425, 1476–1487.

Saio, T., Guan, X., Rossi, P., Economou, A., and Kalodimos, C.G. (2014). Structural basis for protein antiaggregation activity of the trigger factor chaperone. Science 344, 1250494.

Schreiber, G., and Fersht, A.R. (1993). Interaction of barnase with its polypeptide inhibitor barstar studied by protein engineering. Biochemistry 32, 5145–5150.

Schreiber, G., Haran, G., and Zhou, H.-X. (2009). Fundamental aspects of protein-protein association kinetics. Chem. Rev. 109, 839–860.

Selzer, T., and Schreiber, G. (1999). Predicting the rate enhancement of protein complex formation from the electrostatic energy of interaction. J. Mol. Biol. 287, 409–419.

Shoemaker, B.A., Portman, J.J., and Wolynes, P.G. (2000). Speeding molecular recognition by using the folding funnel: the fly-casting mechanism. Proc. Natl. Acad. Sci. USA 97, 8868–8873.

Stull, F., Koldewey, P., Humes, J.R., Radford, S.E., and Bardwell, J.C.A. (2016). Substrate protein folds while it is bound to the ATP-independent chaperone Spy. Nat. Struct. Mol. Biol. 23, 53–58.

Unni, S., Huang, Y., Hanson, R.M., Tobias, M., Krishnan, S., Li, W.W., Nielsen, J.E., and Baker, N.A. (2011). Web servers and services for electrostatics calculations with APBS and PDB2PQR. J. Comput. Chem. 32, 1488–1491.

Vijayakumar, M., Wong, K.Y., Schreiber, G., Fersht, A.R., Szabo, A., and Zhou, H.X. (1998). Electrostatic enhancement of diffusion-controlled protein-protein association: comparison of theory and experiment on barnase and barstar. J. Mol. Biol. 278, 1015–1024.

von Hippel, P.H., and Berg, O.G. (1989). Facilitated target location in biological systems. J. Biol. Chem. 264, 675–678.

Wallis, R., Moore, G.R., James, R., and Kleanthous, C. (1995). Protein-protein interactions in colicin E9 DNase-immunity protein complexes. 1. Diffusion-controlled association and femtomolar binding for the cognate complex. Biochemistry 34, 13743–13750.

Whittaker, S.B.-M.M., Spence, G.R., Günter Grossmann, J., Radford, S.E., and Moore, G.R. (2007). NMR analysis of the conformational properties of the trapped on-pathway folding intermediate of the bacterial immunity protein Im7. J. Mol. Biol. 366, 1001–1015.

Wright, P.E., and Dyson, H.J. (2009). Linking folding and binding. Curr. Opin. Struct. Biol. 19, 31–38.

Zhou, H.X. (2001). Disparate ionic-strength dependencies of on and off rates in protein-protein association. Biopolymers 59, 427–433.

Zhou, H.-X. (2003). Association and dissociation kinetics of colicin E3 and immunity protein 3: convergence of theory and experiment. Protein Sci. 12, 2379–2382.